Selective hydrogenolysis of xylitol to ethylene glycol and propylene glycol over copper catalysts

CrossMark

Zhiwei Huang [a,b,c], Jing Chen [b,c], Yuqing Jia [a], Hailong Liu [b],
Chungu Xia [b,c,**], Haichao Liu [a,*]

[a] Beijing National Laboratory for Molecular Sciences, College of Chemistry and Molecular Engineering, Peking University, Beijing 100871, China
[b] State Key Laboratory for Oxo Synthesis and Selective Oxidation, Lanzhou Institute of Chemical Physics, Chinese Academy of Sciences, Lanzhou 730000, China
[c] Suzhou Institute of Nano-Tech and Nano-Bionics, Chinese Academy of Sciences, Suzhou 215123, China

ABSTRACT

Cu—SiO$_2$ catalysts were prepared by homogeneous deposition–precipitation with a wide range of Cu contents (8.8–100 wt%) and Cu particle sizes (2.1–111.1 nm). These catalysts were evaluated in the selective hydrogenolysis of biomass-derived xylitol to ethylene glycol and propylene glycol under the promotion of Ca(OH)$_2$ base. Their catalytic activity and selectivity to the two glycols depended strongly on the Cu particle sizes, which increased with the particle sizes and reached the maximum values at around 20–35 nm. Such size effects are apparently attributed to the effects on the dehydrogenation and hydrogenation activities of the Cu catalysts, and consequently on the xylitol hydrogenolysis pathways, reflecting the structural requirement for the xylitol hydrogenolysis. The effects of the reaction parameters including H$_2$ pressure (0–8.0 MPa), temperature (433–493 K) and pH values (7.0–12.4, adjusted by changing the amount of Ca(OH)$_2$) were examined. These effects confirmed the reaction pathways previously proposed for the xylitol hydrogenolysis to the two glycols, involving the dehydrogenation of xylitol to xylose on Cu as the rate-determining step, followed by the retro-aldol condensation of xylose with Ca(OH)$_2$ to glycolaldehyde and glyceraldehyde, and their subsequent hydrogenation to ultimately form glycols in competition with their side reactions to glycolic acid and lactic acid in the presence of Ca(OH)$_2$. Upon optimizing the reaction conditions (473 K, 6.0 MPa H$_2$ and sufficient Ca(OH)$_2$), nearly 100% xylitol conversion and 54.4% combined selectivity to ethylene glycol and propylene glycol were obtained on Cu—SiO$_2$ with Cu size of 35.7 nm, comparable to those on the previously reported Ni- and Ru- based catalysts. Clearly, this study provides directions for the design of more efficient Cu catalysts and the optimization of the reaction parameters toward the efficient polyol hydrogenolysis into glycols.

© 2013 Elsevier B.V. All rights reserved.

1. Introduction

In the last decade, due to the worldwide energy and environmental problems, the conversion of renewable biomass, in particular, non-edible lignocellulose, to chemicals and fuels has gained increasing attention [1–4]. In this respect, lignocellulose-derived polyols, sorbitol and xylitol, have emerged as the promising building blocks [5–7]. Herein, we report the selective hydrogenolysis of xylitol to ethylene glycol and propylene glycol on copper-based catalysts. Ethylene glycol and propylene glycol are important commodity chemicals widely used as functional fluids

and for the synthesis of polyester resins, fibers, and pharmaceuticals, *etc.* Currently, they are produced in industry by multi-step transformations of non-renewable petroleum-derived ethylene and propylene, respectively.

So far, Ni-, Ru-, Pd- and Pt-based catalysts [7–21] have been explored for the hydrogenolysis of xylitol and sorbitol to propylene glycol and ethylene glycol in the presence of base additives (*e.g.* NaOH and CaO). For example, Banu et al. [11] reported that on Ni–NaY catalysts, sorbitol was hydrogenolyzed to the two glycols with a combined selectivity of 69% at 66% sorbitol conversion at 493 K and 6.0 MPa H$_2$. Upon incorporation of Pt, the selectivity increased to 82% at a slightly lower conversion (59%) under the same conditions. Ye et al. [12] found that using Ce-promoted Ni/Al$_2$O$_3$ catalysts prepared by co-precipitation method, sorbitol conversion of above 90% and selectivity to the two glycols of 55–60% can be generally obtained at 513 K and 7.0 MPa. On a Ni$_2$P/C catalyst in the presence of Ba(OH)$_2$, the two glycols were formed with 71.4% selectivity at 99% conversion in xylitol hydrogenolysis under

* Corresponding author. Tel.: +86 10 6275 4031; fax: +86 10 6275 4031.
** Corresponding author at: State Key Laboratory for Oxo Synthesis and Selective Oxidation, Lanzhou Institute of Chemical Physics, Chinese Academy of Sciences, Lanzhou 730000, China. Tel.: +86 931 4968089; fax: +86 931 4968129.
E-mail addresses: cgxia@lzb.ac.cn (C. Xia), hcliu@pku.edu.cn (H. Liu).

Table 1
Textural properties of the calcined CuO—SiO$_2$ samples with different Cu loadings before and after reduction in H$_2$ at 553 K.

Sample	Cu loading[a] (wt%)	Crystallite size[b] (nm)		S_{BET}[c] (m^2/g)	V_{Pore}[c] (cm^3)	D_{Pore}[c] (nm)	Cu dispersion[d] (%)	S_{Cu}[e] (m^2/g Cu)	d_{Cu}[f] (nm)
		CuO	Cu^0						
10%CuO—SiO$_2$	8.8	10.5	17.8	204.3	1.32	25.8	48.4	314.0	2.1
30%CuO—SiO$_2$	26.6	11.2	17.6	147.2	0.72	19.4	8.5	55.1	11.8
50%CuO—SiO$_2$	44.9	10.8	18.9	114.2	0.55	19.2	6.2	40.2	16.1
70%CuO—SiO$_2$	65.3	10.4	19.5	91.9	0.44	19.0	4.6	31.7	21.7
90%CuO—SiO$_2$	88.0	13.6	22.8	38.3	0.25	26.6	2.8	18.2	35.7
100%CuO	100	19.2	42.7	15.4	0.082	21.5	0.9	5.8	111.1

[a] Obtained from ICP analysis.
[b] The crystallite sizes calculated from the Scherrer equation.
[c] BET method.
[d] Cu dispersion obtained from dissociative N$_2$O adsorption.
[e] Cu surface area measured by dissociative N$_2$O adsorption.
[f] Mean Cu particle size calculated from dissociative N$_2$O adsorption.

relatively mild conditions of 473 K and 4.0 MPa H$_2$ [14]. Zhou et al. [18] used a mesoporous carbon nanofiber-supported Ru catalyst for the sorbitol hydrogenolysis, showing 85.7% sorbitol conversion and 51.3% combined selectivity to ethylene glycol and propylene glycol at 493 K and 8.0 MPa H$_2$. Recently, Sun et al. [19] studied xylitol hydrogenolysis and achieved a combined selectivity of ~61% to the two glycols at nearly 100% xylitol conversion on Ru/C under relatively mild conditions (473 K and 4.0 MPa H$_2$). Apparently, these studies still encounter low yields to the two target glycols, harsh reaction conditions (*e.g.* high reaction temperatures or H$_2$ pressures), or use of noble metals (*e.g.* Ru). However, the basic understandings from these studies on the reaction mechanism and structural requirements for the polyol hydrogenolysis provide us the direction for further improving the hydrogenolysis efficiency.

The hydrogenolysis of xylitol and sorbitol to ethylene glycol and propylene glycol requires selective cleavage of their specific C–C and C–O bonds. Due to their high activity for the C—C bond cleavage, the aforementioned Ni and Ru catalysts have been frequently applied to the hydrogenolysis of xylitol and sorbitol, but they can catalyze the excessive C—C bond scission to form the undesirable byproducts, such as methane, with high selectivities [12,22,23]. In contrast, Cu is known for its high efficiency in hydro-dehydrogenation of C—O bonds and poor activity for cleavage of C—C bonds [23,24], as evidenced from the dominant formation of deoxyhexitols in the sorbitol hydrogenolysis on a Cu—ZnO catalyst under neutral conditions [22]. Such property of the Cu-based catalysts has been revealed more clearly from the intensively studied glycerol hydrogenolysis, showing superior propylene glycol yields compared to those on other catalysts containing Ru and Ni, *etc.* [25–29]. This property appears to meet the requirement for the hydrogenolysis of C$_5$ and C$_6$ polyols to ethylene glycol and propylene glycol, as widely accepted, involving two key steps, *i.e.* dehydrogenation of polyols to the corresponding carbonyl intermediates on metal catalysts, and the subsequent C–C bond cleavage of the intermediates with bases, most likely *via* the retro-aldol condensation mechanism [18–20,30]. These considerations attempted us to examine the Cu catalysts for the xylitol hydrogenolysis in the presence of bases in this work.

Recently, we reported that Cu—SiO$_2$ catalysts exhibit high efficiency in the hydrogenolysis of glycerol to propylene glycol under mild reaction conditions [27,31,32]. Herein, we extended the application of the Cu—SiO$_2$ catalysts to the xylitol hydrogenolysis to ethylene glycol and propylene glycol in the presence of Ca(OH)$_2$. In comparison with other Cu catalysts supported on ZrO$_2$, Al$_2$O$_3$, ZnO, CeO$_2$, MgO and MgAlO$_x$ with different acid-base and redox properties, we found the superior activity and selectivity of the Cu—SiO$_2$ catalysts. We also examined the effects of Cu particle sizes of the Cu—SiO$_2$ catalysts as well as the effects of reaction parameters (*i.e.* temperatures, H$_2$ pressures, and pH values) on the

xylitol hydrogenolysis, leading to our understanding on the structural requirements and reaction pathways for the formation of the two target glycols on the Cu catalysts.

2. Experimental

2.1. Catalysts preparation

CuO—SiO$_2$ precursors were prepared by homogeneous deposition–precipitation by urea hydrolysis in a 150 mL stainless steel autoclave [33]. SiO$_2$ powder was purchased from Alfa Aesar with a BET surface area of ~430 m^2/g and used as obtained. The amount of SiO$_2$ powder was varied to prepare CuO—SiO$_2$ with Cu loadings from 10 to 100 wt%. The concentrations of Cu^{2+} ions and urea were kept at 0.2 and 2.0 mol/L, respectively. Due to the hydrophilic nature of the SiO$_2$ powder, the concentrations of Cu^{2+} and urea were diluted to 0.1 and 1.0 mol/L, respectively, for the preparation of the CuO—SiO$_2$ sample with 10 wt% Cu loading. The solutions were heated to 373 K and maintained at 373 K for 2 h to form precipitates. The precipitates were filtered, thoroughly washed with deionized water and anhydrous ethanol, and treated in ambient air at 393 K overnight and then at 723 K for 3 h. To study the effect of the initial Cu^{2+} concentrations on the surface structures of the ultimate CuO—SiO$_2$ samples, the CuO—SiO$_2$ oxide precursors with a Cu loading of 50 wt% were prepared at 0.05, 0.1, 0.2, 0.4 and 0.6 mol/L of Cu^{2+}. Mixed oxide CuO—MO$_x$ (M = Mg, Zn, Al, Zr and Ce) precursors were prepared by homogeneous coprecipitation of aqueous solutions of Cu(NO$_3$)$_2$·3H$_2$O and M(NO$_3$)$_x$ by urea hydrolysis [28] (all reagents from Beijing Chemicals, AR grade; ZrO(NO$_3$)$_2$ was used for ZrO$_2$) in the autoclave mentioned above. The concentrations of Cu^{2+} ions and M^{x+} ions in the solutions were varied to change the Cu/M atomic ratios by keeping a constant cation (Cu^{2+} + M^{x+}) concentration of 0.2 mol/L. The urea concentrations were kept at 2.0 mol/L in the solutions. The resulting precursors were then washed, dried and calcined under the same condition as that for the CuO—SiO$_2$ precursors. The calcined CuO—SiO$_2$ samples were labeled as yCuO—SiO$_2$, where y represents the nominal Cu loading. The reduced catalysts were correspondingly denoted as yCu—SiO$_2$. The exact Cu loadings in the as-prepared CuO—SiO$_2$ samples were determined by inductively coupled plasma (ICP, Vario EL), as listed in Table 1.

2.2. Catalysts characterizations

X-ray powder diffraction (XRD) patterns of the samples were obtained in the scanning angle (2θ) range of 20–80° on a Rigaku D/MAX-2400 diffractometer using Ni-filtered Cu Kα1 radiation (λ = 1.5406 Å) operated at 40 kV and 100 mA. The crystallite sizes (d) of CuO and Cu in the samples were calculated by the Scherrer equation: $d = k\lambda/\beta_L \cos\theta$, where k is the Debye—Scherrer constant (0.90),

θ is the diffraction angle and β_L is the full width at half maximum [34]. The average crystallite size of CuO was estimated from the average values at CuO $(-1\,1\,1)$ $(2\theta = 35.5°)$ and $(1\,1\,1)$ $(2\theta = 38.8°)$, and the average crystallite size of Cu^0 from the value at Cu $(1\,1\,1)$ $(2\theta = 43.3°)$.

Field-emission scanning electron microscopy (FE-SEM) images were recorded using a Hitachi S4800 instrument operated at an accelerating voltage of 5 kV. Transmission electron microscopy (TEM) images were taken on a Philips Tecnai F30 FEGTEM operated at 300 kV. For TEM measurement, the samples were ultrasonically dispersed in ethanol and then placed on carbon-coated Cu grids. The BET surface area measurements were performed on a Micromeritics Tristar II 3020 instrument at liquid nitrogen temperature. Prior to measurements, the samples were degassed at 573 K for 4 h.

The dispersion and active Cu surface area of the catalysts were determined by dissociative N_2O adsorption–H_2 temperature-programmed reduction (TPR) reverse titration experiments [28,35], which were carried out on a flow unit (TP5000, Tianjin Xianquan). The as-prepared oxide samples (40–100 mg) were first reduced with 5% H_2/N_2 at a flow rate of 40 mL/min and then the temperature was increased to 553 K at a ramping rate of 3 K/min, and maintained at 553 K for 3 h (denoted as bulk TPR). H_2 consumption was continuously monitored by a thermal conductivity detector (TCD). After cooling to 323 K in a He flow (>99.99%, Beijing Huayuan), the reduced samples were exposed to a 5% N_2O/He mixture (50 mL/min, Beijing Huayuan) for 40 min. Afterwards, the resulting oxidized samples underwent the second TPR run at the ramping rate of 3 K/min from room temperature to 553 K (denoted as surface TPR). The metallic copper surface area, average copper particle size and dispersion were calculated by assuming 1.46×10^{19} copper atoms per m^2 and a molar stoichiometry of $N_2O/Cu_s = 0.5$, where Cu_s means the surface copper atoms.

2.3. Catalytic hydrogenolysis of xylitol

Xylitol hydrogenolysis reactions were carried out in a stainless steel autoclave (100 ml) at a stirring speed of 800 rpm. Prior to the reaction, the calcined samples were reduced at 553 K with a flowing 20% H_2/N_2 for 3 h. In a typical run, 40 g of 10 wt% xylitol (99%, Alfa Aesar) aqueous solution, 0.2 g of reduced Cu catalyst and at least 0.3 g of $Ca(OH)_2$ were introduced into the autoclave. Afterwards, the reactor was purged with H_2 (>99.99%, Beijing Huayuan) three times, pressurized with H_2 to 4.0 MPa and then heated to 473 K, which was kept constant during the reaction. The reactant and liquid products were analyzed by gas chromatography (Agilent 7890A GC) with a capillary column SE54 (50 m × 0.25 mm) after silylation with hexamethyldisilazane (HMDS) and trimethylchlorinesilane (TMSCl) (both ≥98.0%, Alfa Aesar) in pyridine (AR, Shantou Xilong Chemical). The gas products were analyzed by gas chromatography (Shimadzu 2010 GC) with a capillary column OV-101 (30 m × 0.25 mm) and a flame ionization detector. Products were also identified on a HP 6890/5793 GC–MS with a HP-5 column. The detected liquid products included ethylene glycol, propylene glycol, glycerol, lactic acid, glycolic acid, threitol, arabitol, and dehydrated pentitols (containing 1,2,5-pentanetriol and 1,2,4,5-pentanetetrols). Only trace amount of gas products, i.e. CH_4 and CO_2, were detected. The xylitol conversion and product selectivity were calculated on a carbon basis and are defined as follows:

$$\text{Conversion} \ (\%) = \frac{\text{mol of reactant charged} - \text{mol of reactant left}}{\text{mol of reactant charged}} \times 100$$

$$\text{Selectivity} \ (\%) = \frac{\text{mol of product} \times \text{C atoms in product}}{(\text{mol of reactant charged} - \text{mol of reactant left}) \times \text{C atom in reactant}} \times 100$$
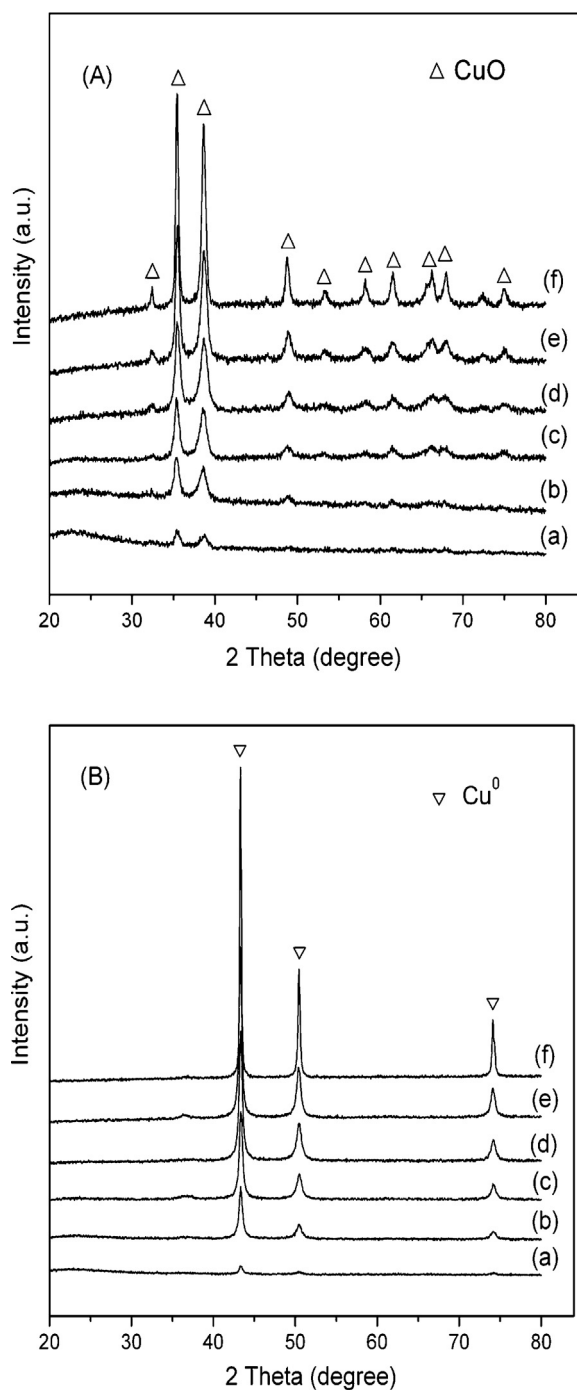

Fig. 1. XRD patterns of the as-prepared CuO—SiO_2 samples (A) and reduced Cu—SiO_2 catalysts (B) with nominal Cu loadings of (a) 10 wt%, (b) 30 wt%, (c) 50 wt%, (d) 70 wt%, (e) 90 wt% and (f) 100 wt%.

3. Results and discussion

3.1. Structural characterization of Cu–SiO_2 catalysts and their precursors

Fig. 1 presents the XRD patterns of the calcined CuO—SiO_2 oxide samples and reduced Cu—SiO_2 catalysts with different Cu loadings. The calcined oxide samples exhibited the characteristic diffractions

of CuO (JCPDS 05-0661, Fig. 1A), which became more intense with increasing the copper content, suggesting the increase in the CuO crystallinity. After reduction at 553 K for 3 h, the CuO peaks disappeared, and the peaks of metallic Cu^0 concurrently appeared at 43.3°, 50.4° and 74.1° (JCPDS 04-0836) even in the catalyst with a 10 wt% Cu loading (Fig. 1B), which were intensified with increasing the copper loading. The mean crystallite sizes of CuO and Cu^0 remained around 10.5 and 18 nm, respectively, almost independent of the Cu loadings up to 70 wt%. Further increase in the Cu loading to 100% resulted in a remarkable increase in the crystallite sizes of CuO and Cu^0 to 19.2 and 42.7 nm, respectively, for the 100%CuO sample before and after reduction (Table 1).

Table 1 shows the textural properties of the calcined CuO–SiO$_2$ samples with different Cu loadings before and after reduction in H$_2$ at 553 K. The BET surface area of the calcined samples decreased from 204.3 m^2/g of 10%CuO–SiO$_2$ to 38.3 m^2/g of 90%CuO–SiO$_2$ with increasing the Cu loading from 8.8 to 88.0%. Pure CuO prepared by the homogeneous precipitation of Cu(NO$_3$)$_2$ by urea hydrolysis possessed a surface area of 15.4 m^2/g. The surface area of pure SiO$_2$ was around 430 m^2/g. The decrease in the surface area of the calcined samples with increasing their copper loadings is apparently due to the decrease in the content of silica support and the coverage of the support surface with CuO. Similarly, the pore volumes of the samples monotonously decreased from 1.32 cm^3/g of 10%CuO–SiO$_2$ to 0.082 cm^3/g of pure CuO. The average pore diameters in the mesopore range for these samples varied in a narrow range 19.0–26.6 nm.

As expected, the CuO–SiO$_2$ samples with lower copper loadings after reduction in H$_2$ possessed higher Cu dispersions measured by N$_2$O chemisorption, which sharply declined from 48.4% of 10%CuO–SiO$_2$ to 8.5% of 30%CuO–SiO$_2$, and then gradually to 2.8% of 90%CuO–SiO$_2$. The Cu dispersion for pure Cu was 0.9%. It is noted that 10%CuO–SiO$_2$ possessed a much higher Cu dispersion (48.4%), which may be not only due to its lower Cu loading, but also to its lower initial concentration of Cu(NO$_3$)$_2$ (0.1 mol/L) than the concentration (0.2 mol/L) used for preparing the other samples. To examine such concentration effect, 50%CuO–SiO$_2$ was prepared at varying Cu(NO$_3$)$_2$ concentrations in the range 0.05–0.6 mol/L, and the Cu dispersion inversely changed from 27.1 to 4.2%, as shown in Table S1 and Fig. S1 (see ESI). With increasing the Cu loadings in the range of 8.8–100 wt%, the Cu surface areas of the Cu catalysts monotonously declined from 314.0 to 5.8 m^2/g, and accordingly their average sizes increased from 2.1 to 111.1 nm. In comparison of these Cu sizes with their XRD results, at Cu loadings below 44.9 wt%, the Cu^0 particle sizes measured by N$_2$O chemisorption were smaller than the values obtained from the XRD results while the Cu sizes measured by N$_2$O chemisorption became larger at the Cu loadings above 65.3 wt% (Table 1). Such discrepancy may be due to the fact that the XRD technique can hardly not only detect very small crystallites (e.g. <3 nm), but also distinguish the primary nanoparticles from their aggregates. In contrast, the N$_2$O chemisorption method provides more reliable values of average sizes for metal particles [36–38]. Such discrepancy also indicates a bimodal distribution of the Cu particles in the Cu–SiO$_2$ catalysts. At Cu loading below 26.6 wt%, the catalysts possessed highly dispersed Cu^0 particles as the major Cu^0 particles, which were below the XRD detection limit, whereas large Cu^0 aggregates, which were detected by XRD, existed in a small amount. With increasing the Cu loading, the dispersed Cu^0 particles tended to aggregate to form the large Cu^0 particles, as evidenced from the following SEM and TEM characterization.

Fig. 2 presents the SEM photographs of the calcined CuO–SiO$_2$ samples with different Cu loadings. It can be seen that 10%CuO–SiO$_2$ consisted mainly of dispersed nanoparticles (Fig. 2a) although it is hard to discriminate between the CuO nanoparticles and silica support. Ribbon-like CuO particles with diameters of about 50–200 nm and lengths of up to 1 μm were also occasionally

observed in this sample. Both CuO nanoribbons randomly separated by SiO$_2$ and CuO particles supported on SiO$_2$ were present in the 30%CuO–SiO$_2$ sample. At Cu loadings above 44.9 wt%, CuO nanoribbons were mainly formed, and their amount increased with increasing the Cu content. Additionally, the nanoribbons were wider and longer at the higher Cu loadings, and they reached ca. 60–700 nm wide and 10 μm long in the Cu-rich 90%CuO–SiO$_2$ and 100%CuO samples. Together with the CuO nanoribbons, dispersed nanoparticles were still present even in the 90%CuO–SiO$_2$ sample (inset of Fig. 2e). After reduction in H$_2$ at 553 K for 3 h, as shown in Fig. S2 (see ESI), the Cu particles largely retained the morphologies of their oxide precursors, as also observed from the following TEM images.

Figs. 3 and 4 show the representative TEM images of the calcined and reduced samples with three Cu loadings of 8.8, 44.9 and 88.0 wt%, respectively. It is clear that the higher Cu loadings led to the formation of more CuO nanoribbons (Fig. 3), which appear to be constructed by the CuO subunit nanoparticles with average diameters of ca. 20–30 nm, as displayed by the high-magnification TEM image in Fig. 3d. After reduction, the Cu particles were formed, and essentially retained the morphologies of the CuO precursors (Fig. 4). The high-magnification TEM image for the reduced 10%Cu–SiO$_2$ catalyst (Fig. 4d) clearly shows that small Cu particles of ca. 2–3 nm were highly dispersed on the SiO$_2$ support, which were still present even in the reduced 90%Cu–SiO$_2$ catalyst. Taken together, these SEM and TEM findings, consistent with the results of XRD and N$_2$O chemisorption (Table 1), show the bimodal distribution of the Cu nanoparticles in the reduced Cu–SiO$_2$ catalysts.

3.2. Xylitol hydrogenolysis activity and selectivity on different copper catalysts

Table 2 shows the conversions and selectivities of xylitol hydrogenolysis at 473 K and 4.0 MPa H$_2$ on seven different supported copper catalysts with similar Cu loadings of ca. 26 wt%. The supports included MgO, SiO$_2$, ZrO$_2$, ZnO, Al$_2$O$_3$, CeO$_2$ and MgAlO$_x$ with different surface acid-basicity and reducibility. The crystallite sizes of their Cu particles were in the range of ca. 15–25 nm, except for Cu/ZrO$_2$ (40.3 nm) before the xylitol hydrogenolysis. The identified products mainly included ethylene glycol, propylene glycol, glycerol, lactic acid, glycolic acid, threitol, arabitol, and dehydrated pentitols. As shown in Table 2, Cu–SiO$_2$ was more active and selective for the formation of ethylene glycol and propylene glycol compared with the other catalysts. After 2 h at 473 K and 4 MPa H$_2$, Cu–SiO$_2$ provided a 28.9% xylitol conversion and a 38.9% selectivity to ethylene glycol and propylene glycol, the highest selectivity to the two target glycols among the seven catalysts examined. Moreover, this catalyst was stable and recyclable. After recycling three times, there was no significant decline in the xylitol conversion and selectivity to glycols (Table 2). This is consistent with the stability of its Cu particles, which became slightly larger after the first run of reaction (17.6 vs. 20.1 nm), and only increased to 24.1 nm after the three successive runs. Cu–MgO exhibited the highest activity and a moderate selectivity to glycols, but its stability was rather poor, and the Cu particles sintered seriously from 24.8 nm to 36.5 nm even after a single run (Table 2). These results show that SiO$_2$ is superior to the other oxide supports for the Cu catalysts in the xylitol hydrogenolysis to the target glycols although the underlying reasons for such support effects need to be clarified, which is clearly not due to their effects on the Cu crystallite sizes, as shown in Table 2.

On these Cu catalysts, the selectivities to acid byproducts, mainly lactic acid and glycolic acid, were very high, in the range of 20–35%, similar to those previously reported on the supported Ru catalysts in the presence of Ca(OH)$_2$ [19]. The selectivities to threitol, the only C$_4$ polyol detected, were always below 1%, lower than
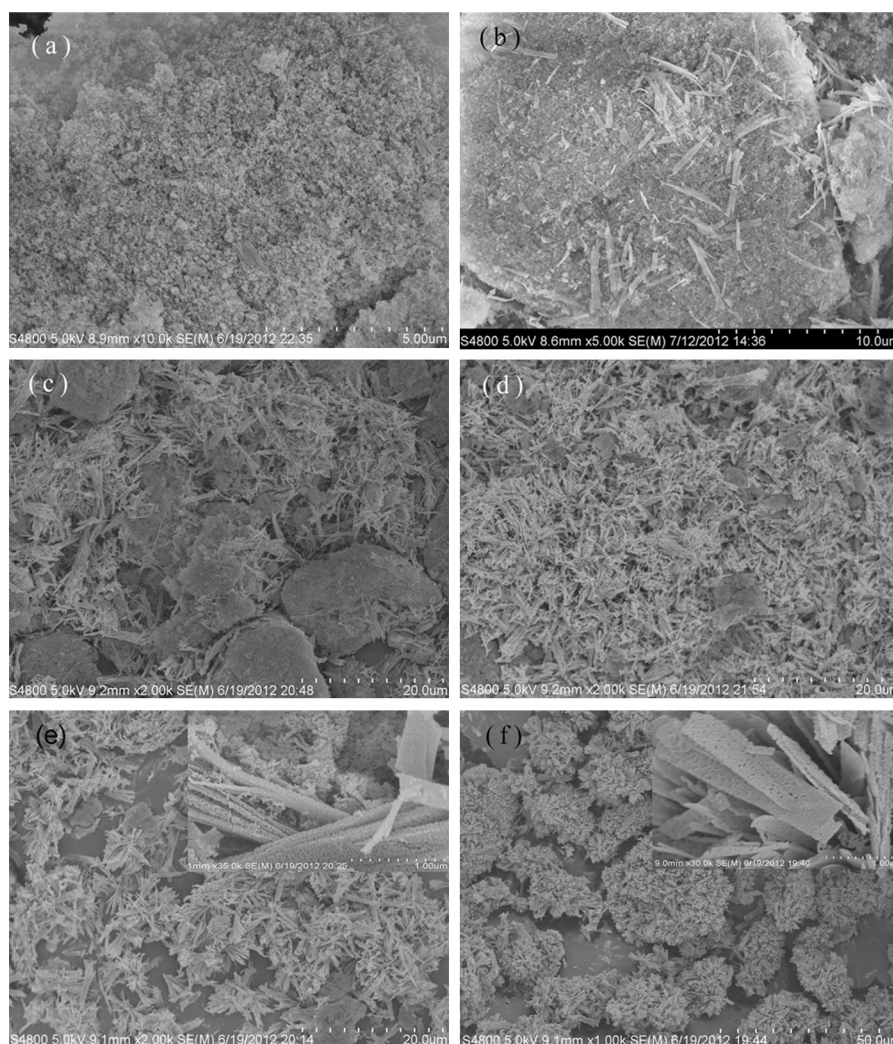
Fig. 2. SEM photographs of the calcined CuO—SiO$_2$ samples with different Cu loadings: (a) 10%CuO—SiO$_2$, (b) 30%CuO—SiO$_2$, (c) 50%CuO—SiO$_2$, (d) 70%CuO—SiO$_2$, (e) 90%CuO—SiO$_2$ and (f) 100%CuO. The scale bar for the inset figures in (e) and (f) is 1 μm.

those (>2%) on the Ru catalysts under the similar reaction conditions [19]. Threitol was proposed to form *via* decarbonylation of the xylose intermediate on Ru surface [19,20]. Thus, the lower threitol selectivities on these Cu catalysts reflect their lower activity of the C—C bond scission, as compared to the Ru catalysts, which can also be seen by the negligible formation of CH$_4$ (<0.1%) on the Cu catalysts. Arabitol, an isomer of xylitol, was formed *via* hydrogenation

of the xylose intermediate [39], and its selectivities were around 10%, indicating the high hydrogenation activity of the Cu catalysts even in the presence of the competitive retro-aldol condensation of xylose catalyzed by Ca(OH)$_2$ [19].

The xylitol hydrogenolysis strongly depends on the Cu particle sizes for the Cu—SiO$_2$ catalysts. The different sizes in a wide range 2.1–111.1 nm were obtained by varying the Cu loadings from 8.8

Table 2
Xylitol conversions and selectivities on Cu catalysts supported on different oxides under basic conditions[a].

Catalyst	Crystallite size[c] (nm)		Conversion (%)	Selectivity (%)[b]							
	Reduced	Used		Ethylene glycol	Propylene glycol	Glycerol	Lactic acid	Glycolic acid	Threitol	Arabitol	Dehydrated pentitols
Cu—MgAlO$_x$	14.6	17.9	25.3	11.8	10.2	0.6	20.2	7.8	0.9	11.2	0.9
Cu—ZnO	14.8	19.2	30.8	9.8	11.2	1.8	24.6	9.9	1.0	10.1	1.0
Cu—SiO$_2$	17.6	20.1	28.9	19.4	19.5	4.4	15.6	7.4	0.7	10.6	1.1
Cu—SiO$_2$ [d]	17.6	24.1	23.7	18.6	19.1	5.2	17.1	7.9	0.9	9.4	1.4
Cu—Al$_2$O$_3$	20.9	24.4	26.1	11.1	12.3	1.0	14.0	6.4	0.7	9.4	0.3
Cu—MgO	24.8	36.5	40.9	15.1	17.1	2.5	24.0	9.9	0.8	9.2	0.8
Cu—CeO$_2$	24.8	27.2	10.1	5.3	1.6	1.3	20.5	2.8	0.8	9.1	2.0
Cu—ZrO$_2$	40.3	42.4	15.0	10.0	7.4	1.7	23.4	4.8	0.7	12.3	2.0

[a] Reaction conditions: 473 K, 4.0 MPa H$_2$, 0.2 g reduced catalyst, 0.3 g Ca(OH)$_2$, 40 g 10 wt% xylitol aqueous solution, 2 h.
[b] The selectivities to light products such as monohydric alcohols and some unidentified products were not shown.
[c] Crystallite sizes of Cu^0 calculated from the Scherrer equation.
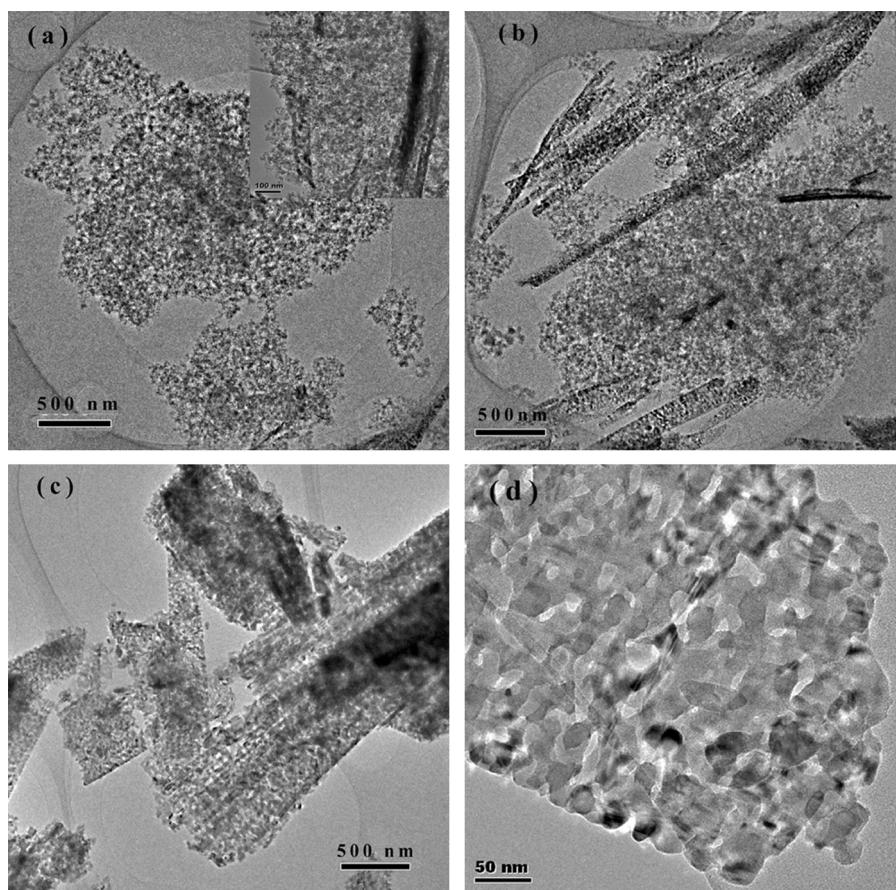[d] After recycling three times.

Fig. 3. TEM images of the calcined CuO—SiO$_2$ samples with different Cu loadings: (a) 10%CuO—SiO$_2$, (b) 50%CuO—SiO$_2$, (c) 90%CuO—SiO$_2$ and (d) higher magnification TEM image of an individual CuO ribbon of 90%CuO—SiO$_2$.

to 100% and initial Cu(NO$_3$)$_2$ concentrations from 0.05 to 0.6 mol/L. Fig. 5 shows the intrinsic activities and selectivities as a function of the Cu particle sizes in the xylitol hydrogenolysis. The intrinsic activity, *i.e.* turnover frequency (TOF), was normalized by the number of surface Cu atoms estimated by N$_2$O chemisorption, as shown in Table 1 and S1. The activities and selectivities were compared at similar xylitol conversions of approximately 30% in the presence of excessive amount of Ca(OH)$_2$. As shown in Fig. 5, the TOFs increased drastically from 12.3 h^{-1} to 123.1 h^{-1} with increasing the Cu particle size from 2.1 nm for 10%Cu—SiO$_2$ to ~21 nm for 50%Cu—SiO$_2$ (prepared using a 0.4 mol/L Cu(NO$_3$)$_2$ concentration shown in Table S1), which then decreased to 97.4 h^{-1} by further increasing the Cu particle sizes to 111.1 nm for the 100% Cu catalyst. It has been proposed that the xylitol hydrogenolysis proceeds by its dehydrogenation to xylose as the rate-determining step [19]. Accordingly, the observed effects of the Cu particle sizes on the TOFs can be attributed to the effects on the dehydrogenation activity of the Cu surfaces. Such effects imply that the xylitol dehydrogenation requires larger Cu domains that are more reactive than the smaller ones, which are similar to those observed for the dehydrogenation of methanol and 2-butanol on the Cu catalysts [37,40], and also for the acetone hydrogenation [41] on the Cu catalysts.

Similar to the change in the TOFs, the combined selectivities to the C$_2$ and C$_3$ polyols, ethylene glycol, propylene glycol and glycerol, also remarkably increased from 18.0% to a maximum value of 43.8% with increasing the Cu particle size from 2.1 nm for 10%Cu—SiO$_2$ to 35.7 nm for 90%Cu—SiO$_2$, which then slowly declined to 39.2% at 111.1 nm for the 100%Cu catalyst (Fig. 5). These C$_2$ and C$_3$ products are derived, according to the proposed xylitol hydrogenolysis mechanism [19], from glycolaldehyde and

glyceraldehyde intermediates that are formed involving the kinetically relevant dehydrogenation of xylitol to xylose on the metal surfaces, and the subsequent retro-aldol condensation of xylose with bases. The increase in the combined selectivities to the C$_2$ and C$_3$ polyols with increasing the Cu particle sizes indicates that the larger Cu particles possess higher hydrogenation activity, and thus facilitate the hydrogenation of the glycolaldehyde and glyceraldehyde intermediates, which would otherwise react to form glycolic acid and lactic acid under the basic conditions [19]. This is indeed consistent with the concurrent decrease in the combined selectivities to lactic acid and glycolic acid with increasing the Cu particle sizes, as shown in Fig. 5. Taken together, the above effects on the TOFs and selectivities show the structure-sensitive nature of the xylitol hydrogenolysis on the Cu catalysts.

Among these catalysts, 90%Cu—SiO$_2$ was very active and exhibited the highest selectivity to ethylene glycol and propylene glycol compared at ~30% xylitol conversion (Table S1 and Fig. 5). It is noteworthy that the higher selectivities to the two target glycols can be obtained at the higher xylitol conversions, as shown in Fig. 6. At 473 K and 4.0 MPa H$_2$, the selectivities to propylene glycol increased from 16.2 to 27.6% with increasing the xylitol conversion from 12.8 to 98.4%, while the selectivities to ethylene glycol increased slightly from 18.3 to 21.8%. These results indicate the stability of the two glycols under the conditions in this work. As a consequence, the combined selectivity to the two target glycols reached 49.4% at nearly 100% xylitol conversion, corresponding to a ~49% yield, even under such non-optimized reaction conditions, showing the potential ability of the Cu catalysts for selective hydrogenolysis of xylitol to the two glycols. As the xylitol conversion increased from 12.8 to 98.4%, the selectivities to glycerol slightly declined from 6.6 to
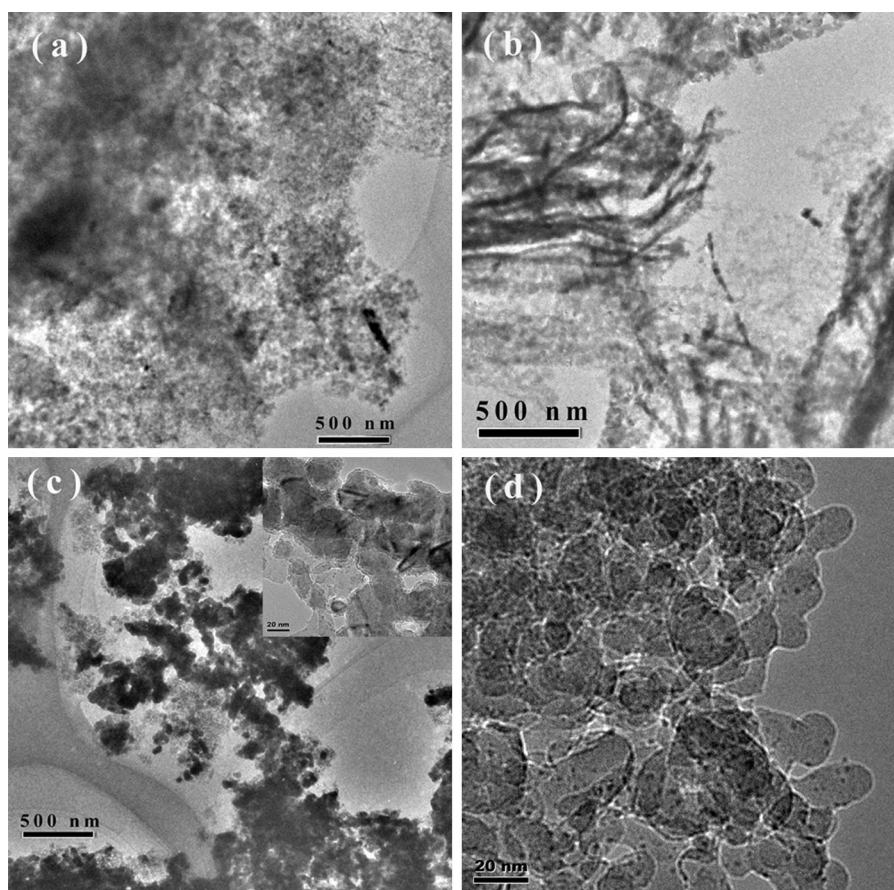
Fig. 4. TEM images of the Cu—SiO₂ catalysts with different Cu loadings reduced at 553 K for 3 h: (a) 10%Cu—SiO₂, (b) 50%Cu—SiO₂, (c) 90%Cu—SiO₂ and (d) high-magnification TEM image of 10%Cu—SiO₂.

2.4% with the concurrent increase in the selectivities to lactic acid from 14.2 to 17.9%, indicating that they may be formed competitively from the same intermediates or lactic acid is formed *via* secondary glycerol reactions in the presence of base [19]. Although glycerol can convert *via* its secondary reactions to propylene glycol over the Cu catalysts in the presence of H_2, as extensively reported previously [25,27–29], and also as our separate glycerol reaction confirmed, the slighter decline in the glycerol selectivities with increasing the xylitol conversion suggests that the larger increase in the propylene glycol selectivities is contributed not solely from the secondary reactions of glycerol, but from the conversion of their same reaction intermediates, *e.g.* glyceraldehyde. The selectivities
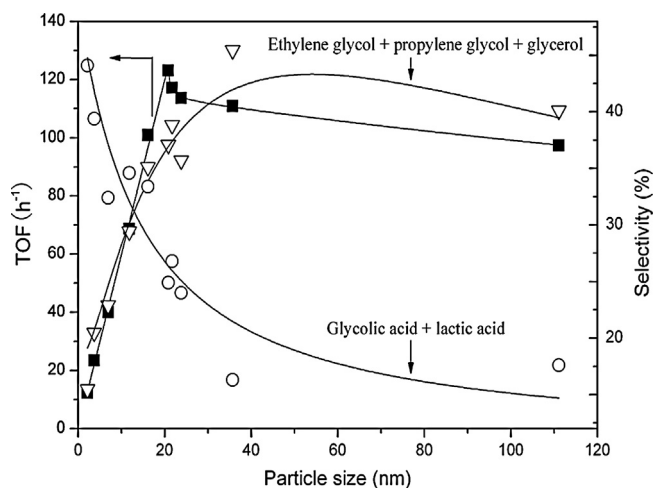

Fig. 5. Dependence of turnover frequencies and combined selectivities to C_2 and C_3 polyols and to acid byproducts in xylitol hydrogenolysis at *ca.* 30% conversion on Cu particle sizes for Cu–SiO₂ catalysts prepared with different Cu loadings and $Cu(NO_3)_2$ concentrations. Reaction conditions: 473 K, 4.0 MPa H_2, 0.043–0.317 g Cu, 0.6–1.2 g Ca(OH)₂, 40 g 10 wt% xylitol aqueous solution, 2 h.
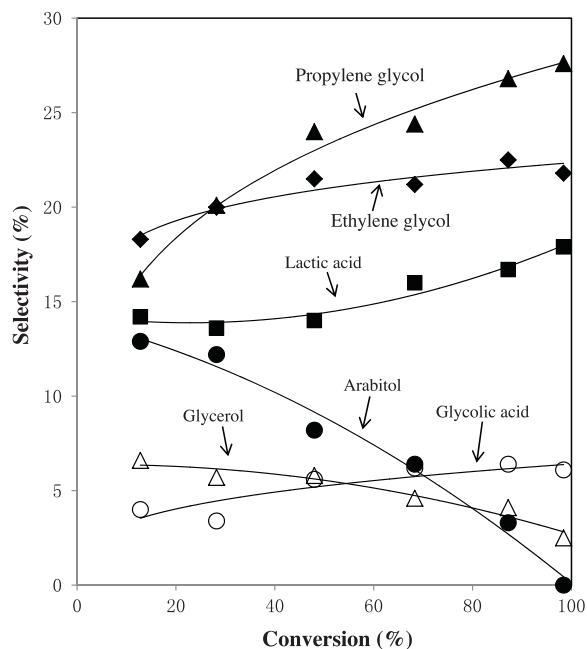

Fig. 6. Dependence of product selectivities on xylitol conversion for 90%Cu—SiO₂ catalyst. Reaction conditions: 473 K, 4.0 MPa H_2, 0.144–0.288 g Cu, 0.4–1.0 g Ca(OH)₂, 40 g 10 wt% xylitol aqueous solution, 0.1–6 h.

Table 3
Effect of the amount of Ca(OH)$_2$ on conversions and selectivities in xylitol hydrogenolysis on 90%Cu–SiO$_2$[a].

Base (mmol)	pH[b]	Conversion (%)	Selectivity (%)						
			Ethylene glycol	Propylene glycol	Glycerol	Lactic acid	Glycolic acid	Arabitol	Adonitol
–	7.0 (5.2)	5.8	4.6	1.7	1.0	Trace	Trace	50.8	7.3
0.5	11.7 (5.9)	15.7	12.2	9.0	4.1	4.5	1.8	39.6	2.7
1.0	11.9 (6.1)	23.8	14.9	12.7	5.2	7.5	2.6	27.1	0.5
2.0	12.1 (6.7)	33.2	18.5	17.2	5.8	9.7	3.5	16.8	0.1
4.0	12.3 (7.6)	52.2	21.1	20.8	5.7	14.0	4.5	9.2	Trace
8.0	12.4 (11.9)	55.9	21.1	24.6	5.6	16.8	4.6	7.3	Trace
16.0	12.4 (12.3)	58.1	21.4	21.9	5.6	19.8	4.7	7.0	n.d.

[a] Reaction conditions: 473 K, 4.0 MPa H$_2$, 0.144 g Cu, 40 g 10 wt% xylitol aqueous solution, 2 h.
[b] Data outside and inside parentheses are pH values measured at 298 K before and after hydrogenolysis reaction, respectively.

to glycolic acid changed in a similar trend to that for ethylene glycol, which increased slightly from 4.0 to 6.1% with increasing xylitol conversion in the range of 12.8–98.4%. In contrast, the selectivities to arabitol declined sharply from 12.9% to nearly 0 with increasing the xylitol conversion from 12.8 to 98.4%, apparently as a result of the further hydrogenolysis of arabitol, once it was formed, reflecting its higher hydrogenolysis activity relative to xylitol, as reported by Deutsch et al. on Ru catalysts [20].

3.3. Effects of reaction parameters on xylitol hydrogenolysis to ethylene glycol and propylene glycol

Recently, Sun et al. [19] reported that on the Ru catalysts, the xylitol hydrogenolysis to ethylene glycol and propylene glycol strongly depends on the reaction parameters, *e.g.* pH values of the reaction solutions and H$_2$ pressures. These parameters influence not only the overall hydrogenolysis rate that is limited by the kinetically relevant dehydrogenation of xylitol to xylose on the Ru surface, but also the selectivities to the two target glycols that are dictated by the base-catalyzed retro-aldol condensation of xylose to glycolaldehyde and glyceraldehyde, and their subsequent hydrogenation. These reactions compete with the hydrogenation of the xylose intermediate and the reactions of the glycolaldehyde and glyceraldehyde intermediates with bases [19]. Similar dependence was observed for the Cu catalysts in this work.

Table 3 shows the effects of the amount of Ca(OH)$_2$ on the activity and selectivity of the 90%Cu–SiO$_2$ catalyst in xylitol hydrogenolysis at 473 K and 4.0 MPa H$_2$. When no base was added, the xylitol conversion was 5.8%, and the selectivities to ethylene glycol, propylene glycol and glycerol were very low, totally being only 7.3%. The xylitol epimers, arabitol and adonitol, were detected to be the major products with selectivities of 50.8 and 7.3%, respectively. It is known that polyol epimerization proceeds by its dehydrogenation to the corresponding carbonyl intermediates, followed by the hydrogenation of the intermediates [39]. The predominant formation of the xylitol epimers is consistent with the finding on the Ru catalysts [19], revealing that Cu is active for the xylitol dehydrogenation to xylose and its reversible hydrogenation, but it is essentially inactive for breaking the C—C bonds in xylitol and its derivatives to form ethylene glycol and propylene glycol. In addition, trace amounts of lactic acid and glycolic acid were also detected, which most likely resulted in the observed decrease in the pH value of the reaction solution from ~7.0 to 5.2 after the hydrogenolysis reaction (Table 3).

Addition of Ca(OH)$_2$ base led to significant change in the xylitol conversions and product selectivities (Table 3). With increasing the amount of Ca(OH)$_2$ from 0 to 4.0 mmol, the xylitol conversion increased sharply from 5.8 to 52.2%, and then gradually to 58.1% after further increasing the amount of Ca(OH)$_2$ to 16.0 mmol (in large surplus), following the trend of increase in the pH values of

the reaction solutions from 7.0 to 12.4 (measured at 298 K before the hydrogenolysis reaction). The control experiment carried out in the absence of the Cu catalysts showed no detectable xylitol conversion on Ca(OH)$_2$ under the identical conditions showing the indispensable role of the Cu catalysts in the xylitol hydrogenolysis. Taken together, it appears to be clear that the favored xylitol conversion at the higher pH values is mainly arisen from the promoting effects of the OH$^-$ ions on the retro-aldol condensation of the xylose intermediate, which would be otherwise hydrogenated reversibly to xylitol and thus limit the xylitol dehydrogenation step on the Cu surfaces. Such promoting effects were evidenced clearly from the change in the dominant products from the xylitol epimers to C$_2$ and C$_3$ products (Table 3). With increasing the amount of Ca(OH)$_2$ from 0 to 4.0 mmol, the selectivities to arabitol and adonitol decreased sharply from 50.8 and 7.3% to 9.2% and nearly zero, respectively, and then the selectivities to arabitol slightly declined to 7.0% after the amount of Ca(OH)$_2$ was further increased to 16.0 mmol. Concurrently, the selectivities to propylene glycol and ethylene glycol monotonically increased to 20.8 and 21.1%, respectively, with increasing the amount of Ca(OH)$_2$ from 0 to 4.0 mmol. Upon addition of more Ca(OH)$_2$ (*i.e.* 8.0 and 16.0 mmol), the selectivities to ethylene glycol remained essentially constant (around 21.1%) while the selectivities to propylene glycol varied from 24.8 to 21.9%. The selectivities to glycerol increased to a constant value of ~5.8% in the present of more than 2.0 mmol Ca(OH)$_2$. Differently, the selectivities to glycolic acid and lactic acid increased monotonically from nearly zero to 4.7 and 19.8%, respectively, reflecting their favorable formation at the higher pH values [19]. However, the combined selectivities to the C$_3$ products (*i.e.* propylene glycol, glycerol and lactic acid) and to the C$_2$ products (*i.e.* ethylene glycol and glycolic acid) monotonically increased with increasing the amount of Ca(OH)$_2$ at the expense of the xylitol epimers, apparently as a result of the aforementioned competitive reactions between the hydrogenation of the xylose intermediate and its retro-aldol condensation. It is noted that the selectivity ratios of the C$_2$ products to the C$_3$ products were between 0.63 and 0.69 in the presence of appropriate amounts of Ca(OH)$_2$ (*e.g.* 1.0–4.0 mmol), as shown in Table 3, close to the theoretical value of 2/3 predicted by the retro-aldol condensation mechanism *via* cleavage of the central C$_2$–C$_3$ bond in the xylose intermediate. This cleavage site selectivity was also observed in the following Fig. 7 at appropriate H$_2$ pressures. Such agreement further confirms that for the xylitol hydrogenolysis on the Cu catalysts, the retro-aldol condensation as the dominating C–C bond cleavage route contributes to the formation of the C$_2$ and C$_3$ products including the two target glycols, as reported for other catalysts such as Ru [18–20].

Fig. 7 shows the activities (normalized per Cu atom) and selectivities for the xylitol hydrogenolysis as a function of H$_2$ pressure on 90%Cu–SiO$_2$. At similar xylitol conversions (~30%), the activities increased sharply from 0.5 to 3.7 h^{-1} with increasing the H$_2$ pressure in the range 0–6.0 MPa at 473 K in the presence of Ca(OH)$_2$.
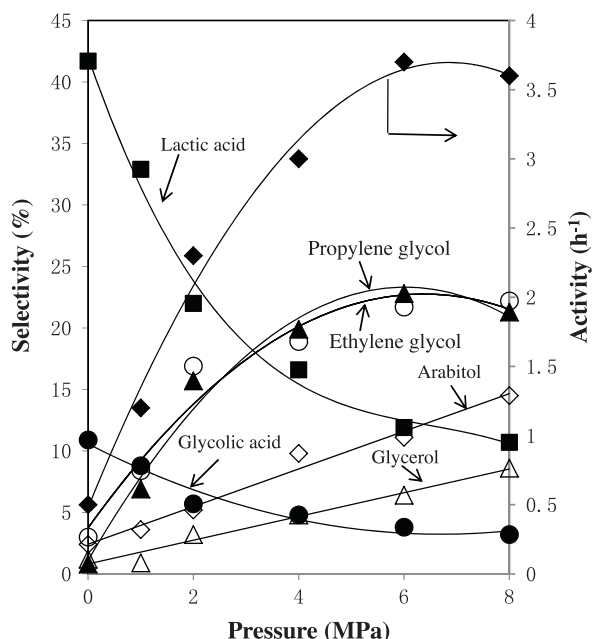
Fig. 7. Effect of H_2 pressure on activities and selectivities for xylitol hydrogenolysis on 90%Cu—SiO_2 at *ca.* 30% conversion. Reaction conditions: 473 K, 0.050–0.187 g Cu, 0.4 g Ca(OH)$_2$, 40 g 10 wt% xylitol aqueous solution, 2 h.

Fig. 8. Effect of temperature on the activities and selectivities for xylitol hydrogenolysis on 90%Cu—SiO_2 at *ca.* 30% conversion. Reaction conditions: 4.0 MPa H_2, 0.0432–0.288 g Cu, 0.4 g Ca(OH)$_2$, 40 g 10 wt% xylitol aqueous solution, 2 h.

Further increasing the H_2 pressure to 8.0 MPa, however, resulted in a slight decrease of the activity to 3.6 h^{-1}, most likely as a consequence of the unfavorable dehydrogenation of xylitol to xylose intermediate against its reversible hydrogenation at such high H_2 pressure [18,19]. Such change is indeed consistent with the linear increase in the selectivities to arabitol with increasing the H_2 pressure in the range 0–8.0 MPa (Fig. 7). Other products also strongly depend on the H_2 pressures. Under inert N_2 atmosphere, the xylitol converted mainly to lactic acid (41.7%) and glycolic acid (10.9%) together with small amounts of ethylene glycol (3.6%), propylene glycol (0.8%), glycerol (1.2%) and arabitol (2.4%). With increasing the H_2 pressure from 0 to 8.0 MPa, the selectivities to lactic acid and glycolic acid sharply decreased from 41.7 to 10.7% and 10.9 to 3.2%, respectively. Concurrently, the selectivities to propylene glycol increased steadily to 22.8% as the H_2 pressure increased to 6.0 MPa H_2, and then slightly decreased to 21.3% at 8.0 MPa H_2, while the selectivities to glycerol increased almost linearly from 1.2 to 8.4% in the whole range 0–8.0 MPa. The selectivities to ethylene glycol increased monotonically from 3.0 to 21.7% with increasing the H_2 pressure from 0 to 8.0 MPa. Such change in the selectivities to the C_2 and C_3 products reflect the higher hydrogenation activities of the 90%Cu—SiO_2 catalyst at the higher H_2 pressures, and the reaction mechanism that they are formed *via* the same intermediates of glyceraldehyde and glycoaldehyde, respectively [19].

The effects of the reaction temperature on the activities and selectivities in the xylitol hydrogenolysis were also examined on 90%Cu—SiO_2. As shown in Fig. 8, at similar xylitol conversions of ~30%, increasing the temperature from 433 to 493 K led to a nearly linear increase in the activities from 0.8 to 5.8 h^{-1}, from which the apparent activation energy was estimated to be 56 kJ/mol. The selectivities to propylene glycol increased with increasing the temperature, and reached the maximum value of ~20% between 453 and 473 K. The selectivities to glycerol monotonically decreased from 7.9 to 3.5% while the selectivities to lactic acid increased significantly from 8.8 to 22.8% with increasing the temperature from 433 to 493 K. Sun et al. [19] also found such favorable formation of lactic acid byproduct at higher temperatures in the hydrogenolysis of xylitol on Ru/C. Such selectivity change for the C_3 products (*i.e.*
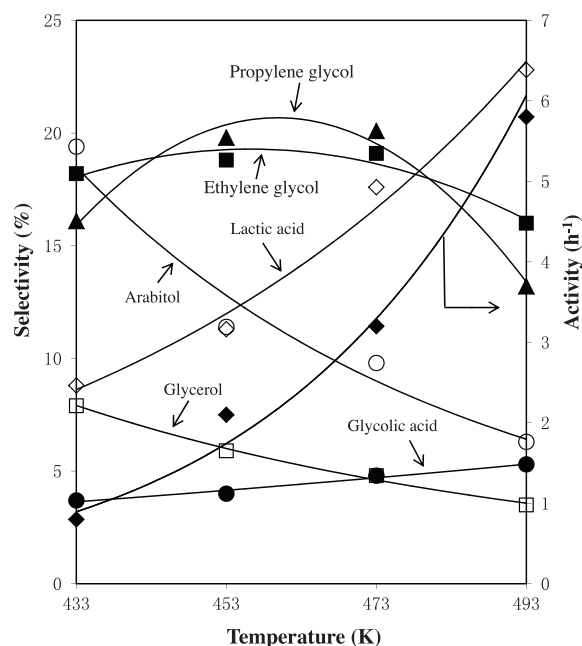
propylene glycol, glycerol and lactic acid) confirmed that they are formed from the same intermediates, as discussed above, which accounts for the decline in the propylene glycol selectivities above 473 K by the favored formation of lactic acid at the higher temperatures. The selectivities to ethylene glycol remained almost constant (around 18.8%) between 433–473 K, and then slightly decreased to 16.0% at 493 K, together with a slight increase in the selectivities to glycolic acid (3.7–5.3%). In contrast, the selectivities to arabitol monotonically decreased sharply from 19.4 to 6.3% in the range 433–493 K. These results demonstrate that the lower temperatures favor the direct hydrogenation of the xylose intermediate on the Cu surfaces while the higher temperatures facilitate the base-catalyzed degradation of this intermediate to C_2 and C_3 products, leading to the efficient synthesis of the target glycols at the appropriate temperatures.

The observed effects of the reaction parameters show the feasibility in improving the efficiency of the xylitol hydrogenolysis. For example, at the appropriate reaction temperatures and H_2 pressures, *e.g.* 473 K and 6.0 MPa H_2, a high xylitol conversion of ~100% and selectivity of 54.4% to ethylene glycol (23.5%) and propylene glycol (30.9%), corresponding to their combined yield of ~54%, were obtained on 90%Cu—SiO_2 in the presence of 12.0 mmol Ca(OH)$_2$, which is comparable to those on the Ni- [10,12] and Ru-based [17–19] catalysts. For example, the combined yield to ethylene glycol and propylene glycol is 61.2% on Ru/C under the similar reaction conditions [19].

4. Conclusions

Cu—SiO_2 catalysts are efficient for the xylitol hydrogenolysis to ethylene glycol and propylene glycol in the presence of Ca(OH)$_2$ as a basic promoter. Their activities and selectivities to the two target glycols depend sensitively on the sizes of the Cu particles in the range of 2.1–111.1 nm, and the Cu particles of around 20–35 nm exhibit the higher efficiency for the synthesis of the two glycols, as a result of their superior dehydrogenation and hydrogenation activities. Such size effects, together with the effects of the reaction temperature, H_2 pressure, and pH value tuned by varying the

amount of Ca(OH)$_2$, are consistent with the reaction pathways previously proposed for the xylitol hydrogenolysis to the two glycols, suggesting that the overall reaction rate is limited by the dehydrogenation of xylitol to the xylose intermediate on Cu while the glycol selectivities rely on the efficient retro-aldol condensation of xylose with Ca(OH)$_2$ to glycolaldehyde and glyceraldehyde, and their subsequent hydrogenation to glycols over their side reactions with Ca(OH)$_2$ to glycolic acid and lactic acid. Notwithstanding that their selectivity and stability need to be further improved, these effects demonstrate the capability of the Cu-based catalysts, with promising potential for substituting the Ni- and noble metal catalysts, for the efficient hydrogenolysis of C$_5$ and C$_6$ polyols to ethylene glycol and propylene glycol.

Acknowledgments

Appendix A. Supplementary data

Supplementary data associated with this article can be found, in the online version, at http://dx.doi.org/10.1016/j.apcatb.2013.09.014.

References

[1] A.J. Ragauskas, C.K. Williams, B.H. Davison, G. Britovsek, J. Cairney, C.A. Eckert, W.J. Frederick Jr., J.P. Hallett, D.J. Leak, C.L. Liotta, J.R. Mielenz, R. Murphy, R. Templer, T. Tschaplinski, Science 311 (2006) 484–489.
[2] A. Corma, S. Iborra, A. Velty, Chem. Rev. 107 (2007) 2411–2502.
[3] D.M. Alonso, J.Q. Bond, J.A. Dumesic, Green Chem. 12 (2010) 1493–1513.
[4] J.C. Serrano-Ruiz, R. Luque, A. Sepúlveda-Escribano, Chem. Soc. Rev. 40 (2011) 5266–5281.
[5] A.M. Ruppert, K. Weinberg, R. Palkovits, Angew. Chem. Int. Ed. 51 (2012) 2564–2601.
[6] J. ten Dam, U. Hanefeld, ChemSusChem 4 (2011) 1017–1034.
[7] R.V. Chaudhari, A. Torres, X. Jin, B. Subramaniam, Ind. Eng. Chem. Res. (2013), http://dx.doi.org/10.1021/ie400709d.
[8] I.T. Clark, Ind. Eng. Chem. 50 (1958) 1125–1126.
[9] M.S.S.R Tanikella, US Patent 4,404,411 (1983).
[10] T.A. Werpy, J.G. Frye, A.H. Zacher, D.J. Miller, US Patent 7,038,094 (2006).
[11] M. Banu, S. Sivasanker, T.M. Sankaranarayanan, P. Venuvanalingam, Catal. Commun. 12 (2011) 673–677.
[12] L. Ye, X. Duan, H. Lin, Y. Yuan, Catal. Today 183 (2012) 65–71.
[13] M. Banu, P. Venuvanalingam, R. Shanmugam, B. Viswanathan, S. Sivasanker, Top. Catal. 55 (2012) 897–907.
[14] T. Soták, T. Schmidt, M. Hronec, Appl. Catal. A 459 (2013) 26–33.
[15] X. Chen, X. Wang, S. Yao, X. Mu, Catal. Commun. 39 (2013) 86–89.
[16] C. Montassier, J.C. Menezo, L.C. Hoang, C. Renaud, J. Barbier, J. Mol. Catal. 70 (1991) 99–110.
[17] J.H. Zhou, M.G. Zhang, L. Zhao, P. Li, X.G. Zhou, W.K. Yuan, Catal. Today 147 (2009) S225–S229.
[18] L. Zhao, J.H. Zhou, Z.J. Sui, X.G. Zhou, Chem. Eng. Sci. 65 (2010) 30–35.
[19] J. Sun, H. Liu, Green Chem. 13 (2011) 135–142.
[20] K.L. Deutsch, D.G. Lahr, B.H. Shanks, Green Chem. 14 (2012) 1635–1642.
[21] B.W. Hoffer, R. Prochazka, WO Patent 2008071642 (2007).
[22] B. Blanc, A. Bourrel, P. Gallezot, T. Haas, P. Taylor, Green Chem. 2 (2000) 89–91.
[23] Z. Wu, Y. Mao, X. Wang, M. Zhang, Green Chem. 13 (2011) 1311–1316.
[24] C. Montassier, J.C. Ménézo, J. Moukolo, J. Naja, L.C. Hoang, J. Barbier, J.P. Boitiaux, J. Mol. Catal. 70 (1991) 65–84.
[25] M.A. Dasari, P.-P. Kiatsimkul, W.R. Sutterlin, G.J. Suppes, Appl. Catal. A 281 (2005) 225–231.
[26] T. Miyazawa, Y. Kusunoki, K. Kunimori, K. Tomishige, J. Catal. 240 (2006) 213–221.
[27] Z. Huang, F. Cui, H. Kang, J. Chen, C. Xia, Appl. Catal. A 366 (2009) 288–298.
[28] S. Wang, Y. Zhang, H. Liu, Chem. Asian J. 5 (2010) 1100–1111.
[29] Z. Yuan, L. Wang, J. Wang, S. Xia, P. Chen, Z. Hou, X. Zheng, Appl. Catal. B 101 (2011) 431–440.
[30] K. Wang, M.C. Hawley, T.D. Furney, Ind. Eng. Chem. Res. 34 (1995) 3766–3770.
[31] Z. Huang, F. Cui, H. Kang, J. Chen, X. Zhang, C. Xia, Chem. Mater. 20 (2008) 5090–5099.
[32] Z. Huang, F. Cui, J. Xue, J. Zuo, J. Chen, C. Xia, Catal. Today 183 (2012) 42–51.
[33] C.J.G. Van Der Grift, P.A. Elberse, A. Mulder, J.W. Geus, Appl. Catal. 59 (1990) 275–289.
[34] R. Jenkins, R.L. Snyder, Introduction to X-ray Powder Diffractometry, John Wiley & Sons, New York, 1996.
[35] C.J.G. Van Der Grift, A.F.H. Wielers, B.P.J. Jogh, J. Van Beijnum, M. De Boer, M. Versluijs-Helder, J.W. Geus, J. Catal. 131 (1991) 178–189.
[36] A.J. Maira, K.L. Yeung, C.Y. Lee, P.L. Yue, C.K. Chan, J. Catal. 192 (2000) 185–196.
[37] E.D. Guerreiro, O.F. Gorriz, G. Larsen, L.A. Arrúa, Appl. Catal. A 204 (2000) 33–48.
[38] A.-P. Jia, S.-Y. Jiang, J.-Q. Lu, M.-F. Luo, J. Phys. Chem. C 114 (2010) 21605–21610.
[39] L. Wright, L. Hartmann, J. Org. Chem. 26 (1961) 1588–1596.
[40] S. Lambert, C. Cellier, F. Ferauche, É.M. Gaigneaux, B. Heinrichs, Catal. Commun. 8 (2007) 2032–2036.
[41] R.S. Rao, A.B. Walters, M.A. Vannice, J. Phys. Chem. B 109 (2005) 2086–2092.